Numerical investigation of the flow in axial water turbines and marine propellers with scale-resolving simulations

Journal of Physics: Conference Series **655** (2015) 012052 doi:10.1088/1742-6596/655/1/012052

Numerical investigation of the flow in axial water turbines and marine propellers with scale-resolving simulations

Mitja Morgut[1], Dragica Jošt[2], Enrico Nobile[2] and Aljaž Škerlavaj[2]

[1] Turboinštitut d.d., Rovšnikova 7, 1210 Ljubljana (Slovenia)

[2] Dipartimento di Ingegneria e Architettura, Università degli Studi di Trieste, via A. Valerio 10, 34127 Trieste (Italy)

E-mail: nobile@units.it

Abstract. The accurate prediction of the performances of axial water turbines and naval propellers is a challenging task, of great practical relevance. In this paper a numerical prediction strategy, based on the combination of a trusted CFD solver and a calibrated mass transfer model, is applied to the turbulent flow in axial turbines and around a model scale naval propeller, under non-cavitating and cavitating conditions. Some selected results for axial water turbines and a marine propeller, and in particular the advantages, in terms of accuracy and fidelity, of Scale-Resolving Simulations (SRS), like SAS (Scale Adaptive Simulation) and Zonal-LES (ZLES) compared to standard RANS approaches, are presented. Efficiency prediction for a Kaplan and a bulb turbine was significantly improved by use of the SAS SST model in combination with the ZLES in the draft tube. Size of cavitation cavity and sigma break curve for Kaplan turbine were successfully predicted with SAS model in combination with robust high resolution scheme, while for mass transfer the Zwart model with calibrated constants were used. The results obtained for a marine propeller in non-uniform inflow, under cavitating conditions, compare well with available experimental measurements, and proved that a mass transfer model, previously calibrated for RANS (Reynolds Averaged Navier Stokes), can be successfully applied also within the SRS approaches.

1. Introduction

CFD has been a useful tool for flow analysis and efficiency prediction of axial turbines and marine propellers for more than 20 years. Regarding water turbines, while the effect of modifications of a runner and other turbine parts on efficiency can be quite accurately estimated, the prediction of absolute efficiency value for different operating regimes is still a challenge. The main problem is an inaccurate flow simulation in a draft tube. RANS models including the SST model, which became a standard in turbo machinery, are not able to model flow in the draft tube accurately. In recent years an intensive research about numerical flow analysis in axial turbines was performed in Turboinštitut [1]. Steady state simulations were done by different turbulence models on grids with different refinements near the walls. At some operating points also transient simulations were done by SST (Shear Stress Transport) and SSG RSM (Reynolds Stress Model) models. On the basis of the results it was concluded, that none of the used turbulence models predicted the efficiency at all operating regimes accurately. With grid refinement some improvements were achieved but the results were still not satisfactory. This was the motivation for time dependent

simulations by more advanced turbulence models, the SAS SST and ZLES. The improvement of results for a Kaplan turbine was presented in [2]. Even greater improvement was achieved in case of a bulb turbine [3]. Recently, in the frame of ACCUSIM project, cavitation prediction and its effect on efficiency of the Kaplan turbine was obtained. Also for the bulb turbine the results were additionally improved by zonal LES model on refined grids [4]. For both turbines a comparison of numerical results to the experimental ones is presented in this paper.
For marine propellers, the predictions of their performances under non-uniform inflow conditions (i.e. wake) and under cavitating conditions is still challenging. In this paper, we will present how a proper combination of a previously calibrated mass transfer model, together with a SAS SST turbulence approach, provides a prediction of the cavitating flow pattern which agrees well with the experimental visualizations.

2. Turbulence models and discretisation schemes

In the analysis reported in this paper, several turbulence models were used: the SST model [5], the SAS SST [6] (hereafter SAS) and the ZLES model [7]. The main idea of the ZLES model is to resolve the flow inside a predefined zone with the LES model, whereas outside the zone a RANS model, either steady or unsteady, is used. At the zone boundaries a Harmonic Flow Generator [8] is used to produce synthetic turbulence. In the simulations of water turbines the zone started just after the interface between the runner and the draft tube, and it is extended to the outlet of the computational domain. Some turbulence models were used in combination with the curvature correction (CC) [9] and with the Kato-Launder limiter (KL) [10] of turbulence production. The CC and KL options were used for water turbines simulations with SST, SAS and ZLES models. In the simulations, we used either 'high resolution' (HRS) or the bounded central difference scheme (BCDS). The high-resolution scheme is a bounded second order upwind biased discretisation, based on the procedure of the Barth and Jespersen's scheme [11]. The bounded central difference scheme (BCDS) is based on the normalised variable diagram and blends from the CDS scheme to the first-order upwind scheme when the convection boundedness criterion [12] is violated. The BCDS was used in combination with SAS and ZLES models, whereas HRS was used in combination with the SST and in order to check the effect of discretisation scheme in some cases also with the SAS turbulence approach.

3. Cavitation and mass transfer models

Cavitating flows can be modelled using several methods. An excellent review of different methods is provided for instance by Koop [13]. In this work we used the homogeneous transport equation based model [14, 15], described in the following.

3.1. Governing equations

As already indicated the cavitating flow is modelled as a mixture of two species i.e. vapour and liquid behaving as a single one, where both phases share the same velocity as well as pressure fields.
In the case of the RANS approach to turbulence, employing the eddy viscosity models and assuming both liquid and vapour phases incompressible, turbulent cavitating flows can be described by the following set of governing equations:

$$\nabla \cdot \mathbf{U} = \dot{m} \left(\frac{1}{\rho_L} - \frac{1}{\rho_V} \right) \tag{1}$$

$$\frac{\partial(\rho \mathbf{U})}{\partial t} + \nabla \cdot (\rho \mathbf{U}\mathbf{U}) = -\nabla P + \nabla \cdot [(\mu + \mu_t)(\nabla \mathbf{U} + (\nabla \mathbf{U})^T)] + S \tag{2}$$

$$\frac{\partial \gamma}{\partial t} + \nabla \cdot (\gamma \mathbf{U}) = \frac{\dot{m}}{\rho_L} \tag{3}$$

which are, in order, the volume continuity and the momentum equation for the liquid-vapour mixture and the volume fraction equation for the liquid phase. In the above equations ρ_L (kg/m^3) and ρ_V (kg/m^3) are the liquid and vapour densities, respectively. $\mathbf{U}$ (m/s) is the averaged velocity and P (Pa) the averaged pressure. S represents the additional momentum sources (for instance the Coriolis and centrifugal forces in the rotating frame of reference). γ is the water volume fraction which is related to the vapour volume fraction α through the volume fraction constraint:

$$\gamma + \alpha = 1 \tag{4}$$

The mixture density ρ (kg/m^3) and laminar dynamic viscosity μ (kg/ms) are evaluated according to:

$$\rho = \gamma \rho_L + (1 - \gamma)\rho_V \tag{5}$$

$$\mu = \gamma \mu_L + (1 - \gamma)\mu_V \tag{6}$$

where μ_L (kg/ms) and μ_V (kg/ms) are the liquid and vapour dynamic viscosities, respectively. $\dot{m}$ $(kg/m^3 s)$ represents the inter-phase transfer rate due to cavitation. In this study $\dot{m}$ was modelled using a mass transfer model briefly presented in the next section.
Finally, in order to close the system of the governing equations, the mixture turbulent viscosity μ_t (kg/ms) was evaluated using one of the turbulence models, developed for the single phase flows, indicated in 2.

3.2. Mass transfer model
The mass transfer model describes/regulates the interphase mass transfer rate due to cavitation. In the past, three different mass transfer models have been considered by the present authors, and their empirical constants have been properly calibrated and validated [16, 17, 18].
Here only the Zwart model, with the calibrated constants, was used, together with a SAS turbulence model.

3.2.1. Zwart model The Zwart model is the native ANSYS CFX mass transfer model. It is based on the the simplified Rayleigh-Plesset equation for bubble dynamics [19]:

$$\dot{m} = \begin{cases} -F_e \dfrac{3 r_{nuc}(1-\alpha)\rho_V}{R_B} \sqrt{\dfrac{2}{3}\dfrac{P_V - P}{\rho_L}} & if\ P < P_V \\ \\ F_c \dfrac{3\alpha\rho_V}{R_B} \sqrt{\dfrac{2}{3}\dfrac{P - P_V}{\rho_L}} & if\ P > P_V \end{cases} \tag{7}$$

In the above equations, P_V is the vapour pressure, r_{nuc} is the nucleation site volume fraction, R_B is the radius of a nucleation site, F_e and F_c are two empirical calibration coefficients for the evaporation and condensation processes, respectively.

4. Improvement of performance prediction for axial turbines with advanced turbulence models

4.1. Efficiency and cavitation prediction for Kaplan turbine
The results of a detailed numerical analysis of flow in a 6-blade Kaplan turbine which operates at middle head are presented. Numerical simulations were done for three angles of runner blades at constant head (see table 1).

Table 1. Local best efficiency points for three angles of runner blades of the Kaplan turbine.

Operating point	β°	φ/φ_{BEP}	ψ/ψ_{BEP}
OP1	12	0.64	0.86
OP2	20	0.95	0.86
OP3	28	1.31	0.86

The turbine consists of semi-spiral casing with two vertical piers, 11 stay vanes and a nose, 28 guide vanes, a 6-blade runner and an elbow draft tube with two vertical piers. Tip clearance was modelled while hub clearance was neglected. The grid in the spiral casing with stay vanes was unstructured, while the grids in the other turbine parts were structured. Near the walls the grids were refined to get recommended values of y^+. For the draft tube and the draft tube prolongation, basic and refined grids were used (table 2). For the other turbine parts, our previous studies [1] showed that with additional refinement only a negligible improvement of results can be obtained. The computational grid for the complete computational domain can be seen in Fig. 1.

Table 2. Number of nodes for the Kaplan turbine parts for the basic grid - BG, and the fine grid - FG.

Turbine part	Number of nodes	
Semi spiral casing with stay vanes		1,480,999
Guide vane cascade		2,755,496
Runner		1,858,374
	BG	FG
Draft tube	1,786,432	6,169,935
Draft tube prolongation	398,056	1,681,992
Total	8,279,357	13,946,796

Detailed results of steady state analysis performed on the basic grid are presented in [2]. At OP1 and OP2 all turbulence models predicted the efficiency values rather well. At OP3, the discrepancy between calculated and measured efficiency values was very large, larger than 4 %. We tried to improve the results at OP3 with transient simulations using SST, SAS and ZLES turbulence models (Fig. 2).

The values of calculated efficiency differ mostly due to different values of flow energy losses in the draft tube and different values of torque. The efficiency value calculated from the steady state solution with SST HRS was 4.42% smaller than the measured one. With transient analysis the results improved significantly. With SST HRS and SAS HRS the efficiency values were smaller than the measured ones by 1.01% and 0.24% respectively. The agreement between measured and numerical values is excellent for SAS BCDS and ZLES BCDS, where the discrepancy is 0.09% and 0.05%, respectively. Based on the results it can be concluded that the SAS and ZLES models with BCDS are suitable for flow simulation at operating points with large discharge. Results obtained by SAS HRS are less accurate mostly due to underestimated torque. Comparing the results of ZLES BCDS on fine and basic grids it was seen that the effect of grid density on the efficiency was negligible. Therefore, for transient simulations for different operating regimes the basic grid was used.

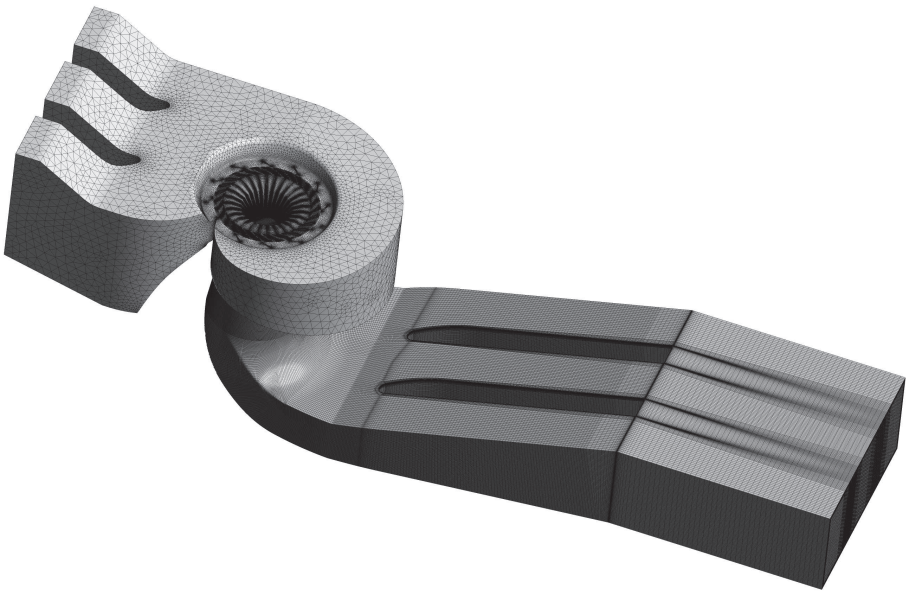

Figure 1. Computational domain and grid for the Kaplan turbine.

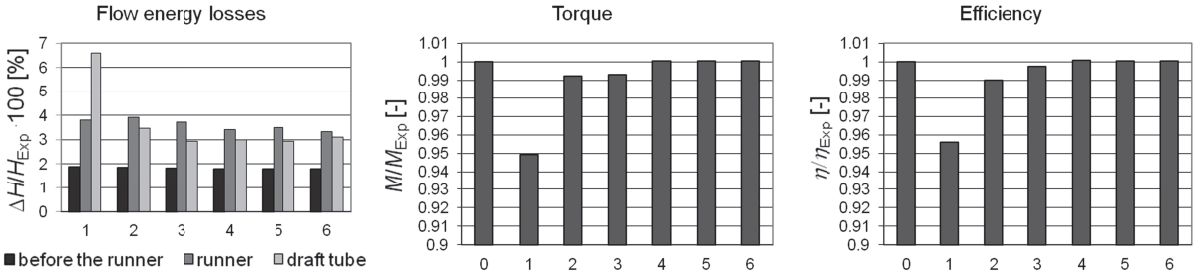

Figure 2. Kaplan turbine - flow energy losses, torque on the shaft and efficiency at OP3. 0 - Experiment; 1 - steady state SST, HRS, FG; 2 - transient SST, HRS, FG; 3 - SAS, HRS, FG; 4 - SAS, BCDS, FG; 5 - ZLES, BCDS, FG; 6 - ZLES, BCDS, BG.

In Fig. 3 flow in the draft tube obtained with steady state SST and transient ZLES is presented. In case of steady state analysis by SST model there is a large swirl at the end of the cone which is by transient simulations nearly completely reduced. Streamlines obtained by the ZLES model are more curled than those obtained by the SST. Vortex structures are represented in Fig. 3(b) and 3(d). By representing viscosity ratio (ratio between eddy and molecular viscosity) it is possible to figure out the amount of modelling in the SST case, and scale-resolving in the ZLES base. By the steady state SST only large vortex structures in the flow were obtained but with the ZLES also small vortex structures were well resolved.

The diagram in Fig. 4 shows a clear distinction between the steady-state simulations and the ZLES, especially at the runner blade angle 28°, where the decrease of calculated flow energy losses in the draft tube was the largest. At the local best efficiency point for runner blade angle 12°(OP1), the calculated and measured values are practically the same. At OP2 (blade angle 20°), the efficiency value obtained with ZLES is about 0.5% smaller than the measured one. The efficiency values at the first three points on the ZLES curve for blade angle 28°agree with the measured results well. At higher discharge, the discrepancy increases. Peak to peak difference

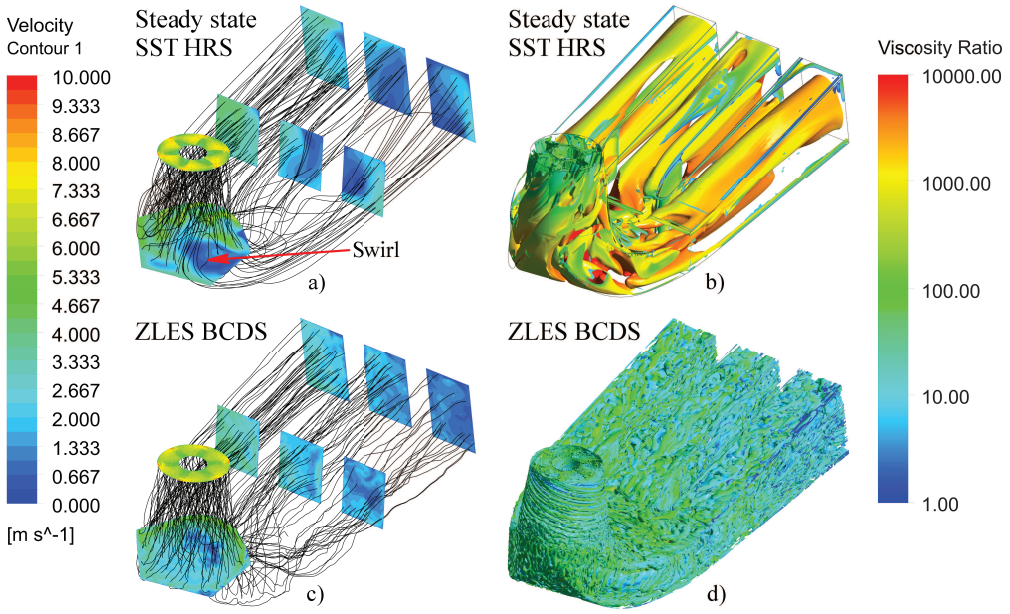

Figure 3. Kaplan turbine - streamlines and velocity contours in the draft tube (left) and isosurfaces of velocity invariant $Q = 0$ (right). Results obtained on fine grid at OP3.

in efficiency values is 0.44% but numerically obtained position of the local best efficiency point is shifted to the left. The tendency that numerical prediction is less accurate at operating points with large discharge still remains, but the improvement with the ZLES model is significant.

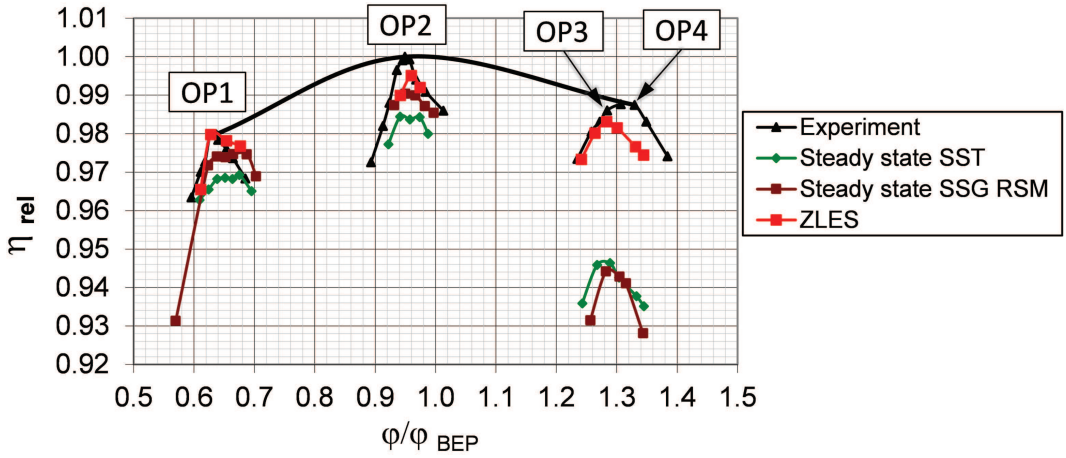

Figure 4. Efficiency diagram for Kaplan turbine - experimental and numerical results.

Cavitation prediction was done at the operating point OP4 (see Fig. 4) because for this point the cavitation was being observed on the test rig and sigma break curve was measured. Two-phase flow simulations are usually less stable, therefore SAS model in combination with robust HR scheme was used instead of ZLES model with BCDS. Cavitating flow was simulated using the homogeneous model. Mass transfer rate due to cavitation was regulated by the Zwart model using vaporization and condensation parameters previously calibrated on a hydrofoil [16, 17].

In order to determine the effect of cavitation on turbine efficiency (sigma-break curve) successive simulations were performed lowering the reference pressure. Steady-state simulations were performed using the MRF (Multiple Reference Frame) approach in combination with the frozen rotor frame/change mixing model. Time-dependent simulations were performed using sliding grids. The first transient simulation that started from steady-state solution was done for non-cavitating conditions. To get the correct flow in the draft tube and stable value of efficiency 20 runner revolutions were needed. For each value of reference pressure three additional runner revolutions were needed.

Numerical results were compared with the observation of cavity size (Fig. 5) on the test rig and with the measured sigma-break curve (Fig. 6). Steady-state simulations did not predict the same extent of cavitation on all blades due to the frozen rotor condition, which somehow preserved differences in circumferential direction. With transient simulation the same amount of cavitation on all runner blades was obtained and the shape and extend of sheet cavitation agreed well with the cavitation observed on the test rig. As already seen in Fig. 4 steady-state simulations significantly under-predicted the efficiency, but the value of sigma, where the efficiency dropped for 1%, agreed well with the experimental result (see Fig. 6). With transient simulations the same amount of cavitation on all runner blades was obtained and the shape and extend of sheet cavitation agreed well with the cavitation observed on the test rig (see Fig. 5). Transient simulations predicted the efficiency more accurately, but the value of sigma where the efficiency dropped for 1% was a bit too large.

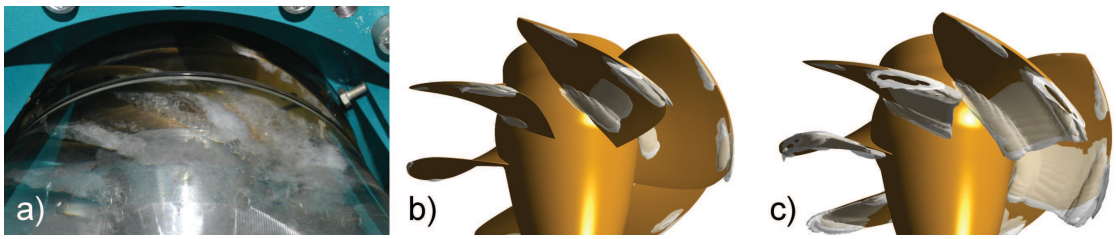

Figure 5. Kaplan turbine - cavity on runner blades: a) observation on test rig, b) steady state simulation, c) time dependent simulation, Th=0.52.

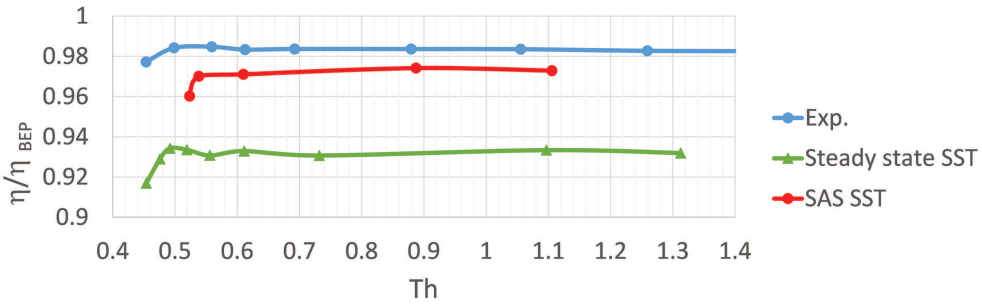

Figure 6. Sigma break curve for Kaplan turbine - experimental and numerical results at OP4.

4.2. Bulb turbine

The bulb turbine considered in this study consists of an inlet part with a vertical pier, 16 guide vanes, 3-blade runner and a draft tube. All simulations were done for a turbine model with

runner diameter D=350 mm. The model was tested on a test rig in accordance with international standard IEC 60193 [20].

Numerical simulations were done for three angles of runner blades and two values of head. The complete results obtained by steady state simulations with the SST turbulence model and by transient simulations with ZLES on the basic grid are presented in [3, 4]. This paper is focused on the local best efficiency point for maximal runner blade angle at smaller head ($\beta = 28°$, $\varphi/\varphi_{BEP} = 1.29$, $\psi/\psi_{BEP} = 0.61$). At this operating regime, the difference between numerical and experimental results was the largest.

To see the effect of grid density on results several computational grids were used (see Tab. 3). The basic grid (BG) with about 9×10^6 nodes is like the grids that are usually used in our simulations. Fine grid 1 (FG1) is in comparison to BG refined only in the draft tube and draft tube extension. FG2 is equal to BG everywhere except in the runner where the grid was refined. FG3 has refined grids in the runner, draft tube and draft tube extension. FG4 is equal to FG1 except in the draft tube and draft tube extension where the grids were additionally refined near walls in order to get for ZLES recommended values of y^+. Coarse grid (CG) with about 2.2×10^6 nodes was used to check whether simulation time could be reduced without too large effect on accuracy of results. The basic computational grid on the whole domain can be seen in Fig. 7.

Due to the frozen rotor condition strong wakes behind the runner blades were obtained and in the region where conical shape of the draft tube changed into a rectangular one a large swirl formed (see Fig. 8(a)). Transient simulations started from the steady state results. During the simulations the swirl was moving towards the outlet and after 22 runner revolutions completely vanished (see Fig. 8(b)).

Comparison of numerical results to the measurements is presented in Fig. 9. Steady state analysis failed to predict efficiency for more than 14% due to overestimated losses in the draft tube and underestimated torque on the shaft. Transient simulations with ZLES significantly improved the results. Positive effect of grid refinement in the draft tube is clearly seen. While with grid refinement in the runner only, no improvement was obtained, the best results were obtained when both grids, in the runner and in the draft tube were refined. In this case (FG3), discrepancy between predicted and measured values of torque on the shaft and turbine efficiency were equal to 1.46% and 2.09%, respectively.

Table 3. Number of nodes in computational grids for bulb turbine

	Inlet part	Guide vane	Runner	Draft tube	Draft tube ext.	Total
Coarse grid	223,375	1,032,976	531,603	211,428	170,332	2,169,714
Basic grid	1,394,720	2,059,568	2,076,603	1,936,188	1,573,336	9,040,415
Fine grid 1	1,394,720	2,059,568	2,076,603	16,324,636	13,176,576	35,032,103
Fine grid 2	1,394,720	2,059,568	6,289,611	1,936,188	1,573,336	13,253,423
Fine grid 3	1,394,720	2,059,568	6,289,611	16,324,636	13,176,576	39,245,111
Fine grid 4	1,394,720	2,059,568	2,076,603	22,292,052	17,885,592	45,708,535

5. Cavitation prediction on a propeller in non-uniform inflow

The numerical predictions of the cavitating E779A model propeller in non-uniform inflow were carried out [21] following the experimental/numerical setup described in [22]. In particular, here, we point out that on the domain Inlet the non-homogeneous inflow (nominal wake), kindly

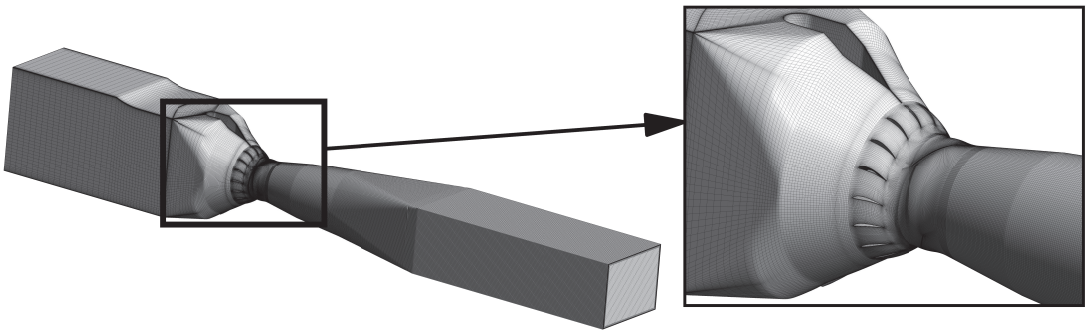

Figure 7. Computational domain and basic grid for bulb turbine.

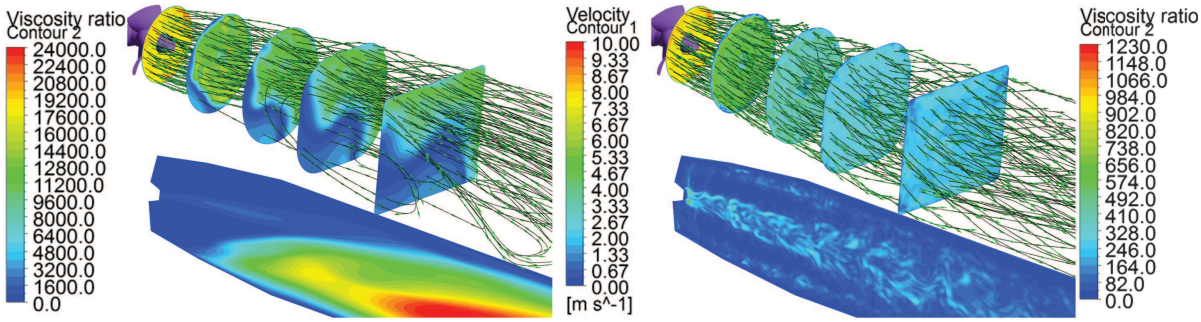

Figure 8. Bulb turbine - flow in the draft tube presented by streamlines and velocity contours, and ratio between eddy viscosity and dynamic viscosity on mid cross-section.

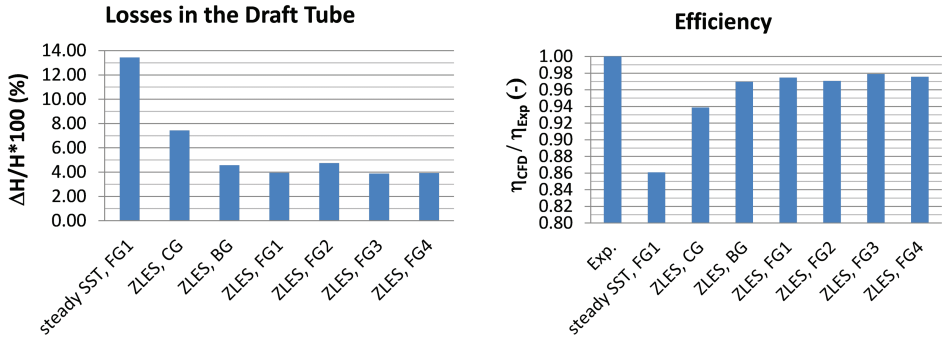

Figure 9. Bulb turbine - comparison of numerical results to the experimental values.

provided by CNR-INSEAN (private communication) was set. On Outlet boundary a fixed value of static pressure was imposed. On the solid surfaces the no-slip wall condition was enforced. The simulated case is schematically presented in Fig. 10. The Fixed domain used a structured numerical grid with 3.3×10^6 nodes, whereas the Rotating domain was meshed as an unstructured hexa-core grid with 7×10^6 nodes. As already described, the cavitation is predicted with the Zwart mass transfer model, with constants previously calibrated on a hydrofoil, using the SAS SST turbulence model. The numerical results agree qualitatively well with the available experimental snapshots describing the cavitation bubble evolution, as reported in figure 11.

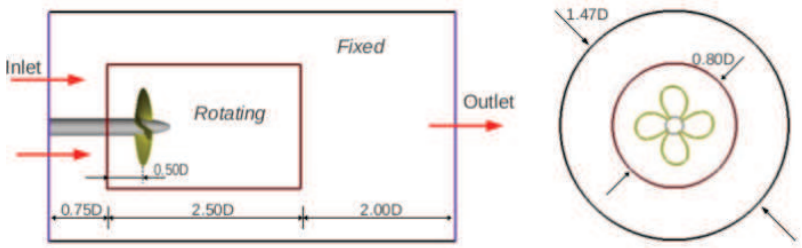

Figure 10. Computational domain for the propeller E779A in non-uniform inflow.

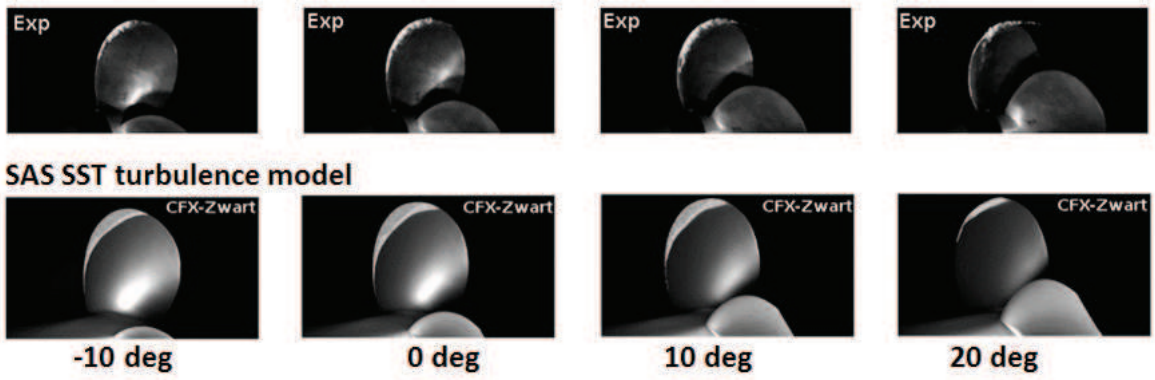

Figure 11. Cavity evolution during propeller rotation. Numerical cavitation patterns depicted using isosurfaces of vapour volume fraction equal to 0.1.

Concluding remarks

On the basis of the detailed analysis of flow in a Kaplan turbine and in a bulb turbine by different turbulence models, and a marine propeller with non-uniform inflow under cavitating conditions, the following conclusions can be drawn:

- For both Kaplan and bulb turbines, it was found out that steady state analysis is not suitable for all operating regimes. While for Kaplan turbine the prediction of efficiency by RANS models was inaccurate only at full rate, for bulb turbine steady state simulations entirely failed. In both cases the main reason for discrepancy between measured and calculated efficiency was the flow in the draft tube, where calculated flow energy losses were overestimated.
- For both turbines the accuracy of results was significantly improved by using ZLES model. For Kaplan turbine the discrepancy was everywhere smaller than 0.8%. For bulb turbine, in spite of large improvement, the discrepancy with measurements was even on the finest grid still 2.09%.
- In the case of the Kaplan turbine the steady-state and time-dependent approaches were compared for the evaluation of the effect of the cavitation on turbine efficiency. The time dependent simulations with SAS SST turbulence model predicted the efficiency more accurately, even though a slightly premature break down of the efficiency was observed.
- In the case of a marine propeller the numerical results, obtained using the SAS SST turbulence approach with a properly calibrated cavitation model, compared qualitatively well with the available experimental data.

Acknowledgments
The research was partly funded by the European Commission - FP7-PEOPLE-2013-IAPP - Grant No. 612279, and by the Slovenian Research Agency ARRS - Contract No. 1000-09-160263.

References
[1] Jošt D and Drešar P 2011 Numerical Analysis of the flow in an axial turbine by different turbulence models (Ljubljana: TurboinÅ¡titut) *Internal report* Nr. 3046 (in Slovene) p 49.
[2] Jošt D Škerlavaj A and Lipej A 2014 Improvement of Efficiency Prediction for a Kaplan Turbine with Advanced Turbulence Models, *J. Mechanical Engineering* **60** 124-34.
[3] Jošt D and Škerlavaj A 2014 Efficiency prediction for a low head bulb turbine with SAS SST and zonal LES turbulence models *IOP Conf. Ser.: Earth Environ. Sci.* **22** 022007.
[4] Jošt D Škerlavaj A Morgut M and Nobile E 2015 Effects of turbulence model and grid resolution on the performance prediction of a bulb turbine. To be presented at *NAFEMS World Congress 2015*, San Diego, USA.
[5] Menter F R Kuntz M and Langtry R 2003 Ten years of industrial experience with the SST turbulence model *Turbulence, Heat and Mass Transfer* 4. ed Hanjalič K Nagano Y and Tummers M (Begell House, New York) pp 625-632.
[6] Egorov Y and Menter F 2008 Development and application of SST-SAS turbulence model in the DESIDER project. *Advances in Hybrid RANS-LES Modelling* ed Peng S -H and Haase W (Springer, Heidelberg), pp 261-270.
[7] Menter, F.R., Gabaruk, A., Smirnov, P., Cokljat, D., Mathey, F 2010 Scale-Adaptive Simulation with Artificial Forcing *Progress in Hybrid RANS-LES Modelling* ed Peng S -H Doerffe P and Haase W (Springer, Berlin) 235-46.
[8] Adamian D and Travin A 2011 An efficient generator of synthetic turbulence at RANS-LES interface in embedded LES of wall-bounded and free shear flows *Computational Fluid Dynamics 2010* ed Kuzmin A (Springer, Berlin) pp 739-744.
[9] Smirnov P E and Menter F 2009 Sensitization of the SST turbulence model to rotation and curvature by applying the Spalart-Shur correction term. *J. Turbomachinery* **131**, no. 4, p 041010.
[10] Kato M and Launder B E 1993 The modelling of turbulent flow around stationary and vibrating square cylinders *Procs 9th Symposium on Turbulent Shear Flows* p 10.4.1-10.4.6.
[11] Barth T J and Jespersen D C 1989 The design and application of upwind schemes on unstructured meshes *27th Aerospace Sciences Meeting* AIAA Paper 89-0366.
[12] Jasak H Weller H.G. and Gosman A D 1999 High resolution NVD differencing scheme for arbitrarily unstructured meshes *Int. J. Num. Meth. Fluids* **31** no. 2 pp 431-449.
[13] Koop A H 2008 Numerical simulation of unsteady three-dimensional sheet cavitation (Ph.D. thesis), University of Twente.
[14] Bouziad Y A 2005 Physical modelling of leading edge cavitation: computational methodologies and application to hydraulic machinery (Ph.D. thesis) Ecole Polytechnique Federale de Lausanne.
[15] ANSYS 2009 *ANSYS CFX-Solver Theory Guide, Release 12.0.*
[16] Morgut M, Nobile E and Biluš I 2010 Comparison of mass transfer models for the numerical prediction of sheet cavitation around a hydrofoil, *Int. J. Multiphase Flow* **37(6)** 620-26.
[17] Morgut M and Nobile E 2012 Numerical Predictions of Cavitating Flow Around Model Scale Propellers by CFD and Advanced Model Calibration, *Int. J. Rotating Machinery* Article ID 618180, 11 pages.
[18] Morgut M and Nobile E 2011 Numerical Predictions of the Cavitating and Non-Cavitating Flow Around the Model Scale Propeller PPTC. *Proc. of the Workshop on Cavitation and Propeller Performance, 2nd International Symposium on Marine Propulsors* (Hamburg, Germany).
[19] Brennen C E 2005 *Fundamentals of Multiphase Flows* (New York, NY, USA Cambridge University Press).
[20] IEC 60193 1999 Hydraulic turbines, storage pumps and pump-turbine - Model acceptance tests. (International Electrotechnical Commission, Geneva).
[21] Morgut M Jošt D Nobile E and Škerlavaj A 2015 Numerical investigations of a cavitating propeller in non-uniform inflow. To appear in *Procs of Fourth International Symposium on Marine Propulsors* (Austin, Texas, USA).
[22] Salvatore F Streckwall H and van Terwisga T 2009 Propeller Cavitation Modelling by CFD-Results from the VIRTUE 2008 Rome Workshop *Proc. of the First International Symposium on Marine Propulsors, smp'09* (Trondheim, Norway).